



HAL
open science

Importance of two-electron processes in Fe-catalyzed aryl-(hetero)aryl cross-couplings: evidence of Fe⁰ / Fe^{II} couple implication.

Vincent Wovk, Lidie Rousseau, Guillaume Lefèvre

► To cite this version:

Vincent Wovk, Lidie Rousseau, Guillaume Lefèvre. Importance of two-electron processes in Fe-catalyzed aryl-(hetero)aryl cross-couplings: evidence of Fe⁰ / Fe^{II} couple implication.. *Organometallics*, 2021, 40 (19), pp.3253-3266. 10.1021/acs.organomet.1c00338 . hal-03426953

HAL Id: hal-03426953

<https://hal.science/hal-03426953v1>

Submitted on 12 Nov 2021

HAL is a multi-disciplinary open access archive for the deposit and dissemination of scientific research documents, whether they are published or not. The documents may come from teaching and research institutions in France or abroad, or from public or private research centers.

L'archive ouverte pluridisciplinaire **HAL**, est destinée au dépôt et à la diffusion de documents scientifiques de niveau recherche, publiés ou non, émanant des établissements d'enseignement et de recherche français ou étrangers, des laboratoires publics ou privés.

Importance of two-electron processes in Fe-catalyzed aryl-(hetero)aryl cross-couplings: evidence of Fe⁰ / Fe^{II} couple implication.

Vincent Wowk,^[a] Lidie Rousseau,^[a,b] and Guillaume Lefèvre^[a]*

[a] Chimie ParisTech, PSL University, CNRS, Institute of Chemistry for Life and Health Sciences, CSB2D, 75005 Paris, France

[b] Université Paris-Saclay, CEA, CNRS, NIMBE, 91191 Gif-sur-Yvette cedex, France

ABSTRACT. We demonstrate in this work that two drastically distinct mechanisms can be involved in aryl-(hetero)aryl Fe-mediated cross-couplings between Grignard reagents and organic halides, depending on the nature of the latter. (Hetero)aryl electrophiles which easily undergo one-electron reduction can be involved in a $\text{Fe}^{\text{II}} / \text{Fe}^{\text{III}}$ coupling sequence featuring an *in situ* generated organoiron(II) species, akin to their aliphatic analogues. On the other hand, less easily reduced substrates can be activated by transient Fe^0 species formed by reduction of the precatalyst. In this case, the coupling mechanism relies on 2-electron elementary steps involving the $\text{Fe}^0 / \text{Fe}^{\text{II}}$ redox couple, and proceeds by an oxidative addition / reductive elimination sequence. Hammett analysis shows that both those elementary steps are faster for electrophiles substituted by electron-withdrawing groups. The two mechanisms discussed herein can be involved concomitantly for electrophiles displaying an average oxidative power. Attesting to the feasibility of the aforementioned bielectronic mechanism, high-spin organoiron(II) intermediates formed by 2-electron oxidative addition onto (hetero)aryl halides in catalytically relevant conditions were also characterized for the first time. Those results are sustained by paramagnetic ^1H NMR, kinetics monitoring, as well as by DFT calculations.

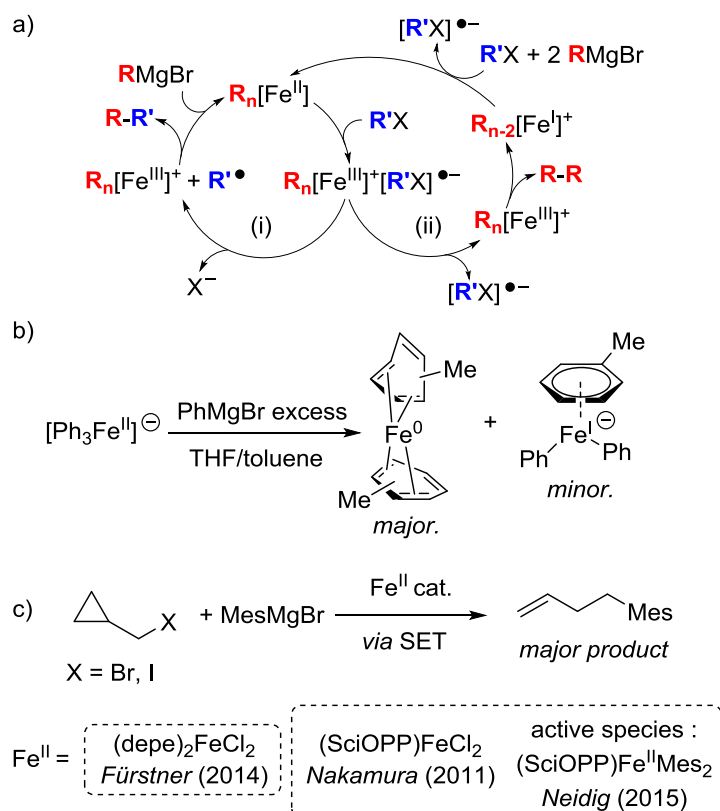
KEYWORDS. iron catalysis • cross-coupling • mechanisms • two-electron processes • kinetics

INTRODUCTION. Fe-catalyzed cross-coupling reactions have been intensely developed in the last decades, thanks to the pioneer work of Kochi,^{1a-b} Cahiez,^{1c} Fürstner,^{1d-e} Nakamura^{1f-g} and Bedford.^{1h-i} Use of this cheap and abundant metal led to a significant breakthrough in transition-metal catalysis; however, despite those significant ecologic and economic advantages,² reaching a fine understanding of the mechanistic facets of the corresponding transformations is still a challenging issue, especially due to the short lifetimes of the active species³ and to the large panel of oxidation states formed under catalytically-relevant coupling conditions.

From a mechanistic standpoint, numerous coupling systems involving aliphatic $\text{C}_{\text{sp}^3}\text{-X}$ electrophiles (X = halide or pseudo-halide) proved to follow a radical pathway, with *in-situ*-generated organoiron(II) intermediates as active species. The key step of the coupling is in that case the activation of the electrophile by the latter in a single-electron transfer step (SET) leading to the generation of an organoiron(III) intermediate

and an organic radical. The coupling proceeds in a second time by a radical rebound of those two intermediates. This general mechanistic pattern is summarized in Scheme 1a (cycle (i)). A classical competitive pathway often limiting the selectivity of the cross-coupling is the homocoupling of the nucleophile, which can usually take place by reductive elimination in a multiple transmetallated organoiron(II) or organoiron(III) intermediate (see Scheme 1a, cycle (ii)).⁴

Scheme 1: a) general scheme of the cross-coupling (i) and homocoupling (ii) catalytic cycles relying on a one-electron process; b) evolution of $[\text{Ph}_3\text{Fe}^{\text{II}}]^-$ towards lower oxidation states; c) examples of mesityl-alkyl cross-couplings proceeding by SET activation of radical clocks; depe = 1,2-(bis)-diethylphosphinoethane; SciOPP = 1,2- $\text{C}_6\text{H}_4((3,5\text{-C}_6\text{H}_3\text{tBu}_2)_2\text{P})_2$.



MesMgBr (Mes = mesityl = 2,4,6- $\text{C}_6\text{H}_2\text{Me}_3$) has been widely used as a mechanistic probe of the implication of Fe^{II} oxidation state in catalytic processes. Transmetalation of an excess of MesMgBr with Fe^{II} or Fe^{III} salts indeed quantitatively leads to the *ate* species $[\text{Mes}_3\text{Fe}^{\text{II}}]^-$ without further reduction of the iron.⁵ Kinetic

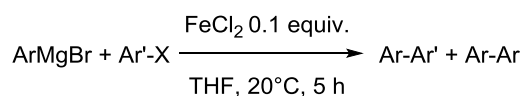
stability of this homoleptic complex is enhanced due to the presence of the methyl substituents in *ortho* position to the metal, preventing any 2-electron reductive elimination to the Fe⁰ stage unlike other sterically less hindered related species such as [Ph₃Fe^{II}]⁻ (Scheme 1b).⁶ Therefore, formation of a cross-coupling product using Fe^{II/III} precatalysts and involving MesMgBr as a nucleophile likely proceeds *via* the formation of a reactive key mesityl-Fe^{II} intermediate, with no further reduction of the metal. A broad variety of iron-catalyzed cross-couplings involving alkyl halides as electrophiles and MesMgBr as nucleophile has been reported in literature, those transformations involving a radical-based mechanism as depicted in Scheme 1a. Amongst relevant examples of such radical-processing couplings, Fürstner demonstrated that MesMgBr could efficiently react with several primary alkyl halides in the presence of bidentate (P,P)- or (N,N)-ligated Fe^{II} catalysts.⁷ Implication of one-electron activation of the alkyl halide was probed by the use of suitable radical clocks (Scheme 1c). A similar work probing radical activation of primary alkyl halides was reported by Nakamura with SciOPP-ligated iron(II) precursors (Scheme 1c);^{8a} in the latter case, Neidig reported that the bis-mesityl complex (SciOPP)Fe^{II}Mes₂ was responsible of the catalytic activity.^{8b}

On the other hand, the state of the art regarding the mechanistic facets of iron-catalyzed couplings involving C_{sp2} aryl or heteroaryl electrophiles remains extremely scarce, although a broad variety of aryl-(hetero)aryl coupling systems promoted by iron catalysts has been described in the last decades.⁹ (Hetero)aromatic halides difficultly undergo activation by single-electron transfer as depicted in Scheme 1a. This is due to the intrinsic instability of the aryl C_{sp2}-centered radicals, which translates into bond dissociation energies of the C_{sp2}-X bonds much higher than those of their aliphatic analogues. For example, bond dissociation energy of the C-I (resp. C-Br) bond at 298 K increases from 55.6 kcal.mol⁻¹ in *t*Bu-I to 67 kcal.mol⁻¹ in Ph-I (resp. from 72.6 kcal.mol⁻¹ in *t*Bu-Br to 84 kcal.mol⁻¹ in Ph-Br).¹⁰ In line with this energetically demanding one-electron activation of (hetero)aryl electrophiles, several two-electron aryl-(hetero)aryl coupling mechanisms have been suggested in the past. For example, Nakamura has reported a cross-coupling between aryl chlorides and aryl Grignard reagents mediated by a NHC-stabilized Fe^{II} catalyst in the presence of fluoride anions, suggesting the activation of the Ar-Cl bond by a Fe^{II} oxidative addition, leading to a Fe^{IV} intermediate.¹¹ We also demonstrated recently that the bis-aryl neutral complex (η⁴-C₆H₅Me)₂Fe⁰, obtained by reduction of FeCl₂ with

PhMgBr in THF:toluene mixtures (Scheme 1b), was able to promote aryl-heteroaryl cross-couplings, associated with a Fe^{II} resting state and thus suggesting the occurrence of a possible Fe⁰ / Fe^{II} catalytic cycle.^{6b} In this work, we demonstrate that a new coupling mechanistic pattern, relying on two-electron elementary steps involving the Fe⁰ / Fe^{II} couple, can be at play in aryl-heteroaryl cross-couplings of aryl Grignards with heteroaryl chlorides. This mechanism involves an activation of the heteroaryl chloride by an *in situ* generated Fe⁰ precursor in a S_NAr-type oxidative addition. In particular, several heteroleptic organoiron(II) complexes formed by oxidative addition of the Fe⁰ precursor onto an (hetero)aryl halide were spectroscopically evidenced. Proficiency of this unprecedented bielectronic mechanism in aryl-heteroaryl cross-coupling is discussed depending on the reduction potential of the heteroaryl chloride. Those data have been probed by paramagnetic ¹H NMR and kinetics analysis, and are supported by DFT calculations.

RESULTS AND DISCUSSION. A representative benchmark of aryl and heteroaryl halides (Ar'-X) used as electrophilic partners in FeCl₂-mediated cross-couplings with MesMgBr and PhMgBr has been investigated. Table 1 gathers the results obtained for 5-substituted 2-chloropyridines (Entries 1-8), 2-chloropyrimidine (Entries 9-10), 2-chloroquinoline (Entries 11-12), C₆F₅Cl (Entry 13-14) and PhI (Entry 15). Cross-coupling (ArAr') and homocoupling (ArAr) yields are displayed (Ar = Mes, Ph). In the latter case, since some PhPh is formed upon reduction of FeCl₂ at lower oxidation states by PhMgBr (see Scheme 1b), a corrected yield is given, which corresponds to the total yield truncated of the quantity of PhPh obtained by adding PhMgBr onto FeCl₂ in the absence of the electrophile.

Table 1: aryl-(hetero)aryl cross-coupling benchmark between ArMgBr (Ar = Mes, Ph) and various (hetero)aryl halides; yields based on GC-MS analysis. [a] corresponds to the overall PhPh yield truncated of 20% which are formed upon reduction of FeCl₂; [b] at 25°C in DMF, see ref. 12a; [c] this work (potentials measured on a Pt disk electrode at 25°C in CH₃CN); [d] in CH₃CN, see ref. 12b; [e] see ref. 12c; [f] in CH₃CN, see ref. 12d; [g] with 5 equiv. TEMPO per mole of iron; [h] in the absence of iron.



Entry	Ar'-X	$E_{\text{red}}(\text{Ar}'\text{-X})$ (V vs SCE)		% Ar-Ar'	% Ar-Ar (corr.) ^[a]
	2-chloro-5-Z-pyridines				
1	Z = H	-2.37 ^[b]	Ar = Mes	0	0
2			Ar = Ph	38	11
3	Z = F	-2.25 ^[c]	Ar = Mes	0	0
4			Ar = Ph	25	18
5	Z = Me	-2.40 ^[c]	Ar = Mes	0	0
6			Ar = Ph	23	12
7	Z = CF ₃	-1.60 ^[c]	Ar = Mes	14 (1) ^[g]	23
8			Ar = Ph	26 (16) ^[g]	25
9	2-chloropyrimidine	-1.96 ^[d]	Ar = Mes	4 (1) ^[g] (2) ^[h]	traces
10			Ar = Ph	15	9
11	2-chloroquinoline	-1.92 ^[e]	Ar = Mes	5	traces
12			Ar = Ph	30	15
13	C ₆ F ₅ Cl	-2.05 ^[f]	Ar = Mes	0	0
14			Ar = Ph	4	65
15	PhI	-1.91 ^[b]	Ar = Mes	5	5

In the conditions described herein (Table 1), some electrophiles proved to react with MesMgBr and to afford cross-coupling product, even in small yields (Entries 7, 9, 11 and 15). Due to the intrinsic *ortho* hindrance of MesMgBr, leading to difficult formation of bisaryl moieties at a transition metal ion, examples of aryl-aryl cross-coupling involving MesMgBr as a nucleophile are much less common than their aryl-alkyl counterparts. Mesityl-aryl couplings thus usually proceed with modest yields, attesting nonetheless to the feasibility of the catalytic process in a certain extent. For example, Huynh and Duong described a NHC-stabilized Fe^{II} catalyst allowing cross-coupling between MesMgBr and *o*-tolyl chloride with a 26 % yield.¹³ The mesityl-hetero(aryl) couplings discussed herein accordingly proceed with modest to low yields when the coupling product is observed: 2-chloro-5-trifluoromethylpyridine led for example to the formation of 14 % of the corresponding coupling product (Entry 7). For this electrophile, 23 % of bisaryl MesMes is also detected. 2-chloropyrimidine, 2-chloroquinoline and iodobenzene also afforded small amounts of mesityl-coupling

products, as well as traces of MesMes (Entries 9, 11, 15). Interestingly, electrophiles which do not afford cross-coupling product with MesMgBr also do not lead to formation of bisaryl MesMes (Entries 1, 3, 5, 13). Conversely, all the investigated substrates led to the expected coupling product when PhMgBr was used (23-38 % yield observed for the 5-Z substituted 2-chloropyridines, Entries 2, 4, 6, 8), as well as to variable quantities of homocoupled bisaryl PhPh. Electron-poor C₆F₅Cl afforded traces of coupling product, mostly leading to homocoupling of PhMgBr (Entry 14).

It is noticeable that, among the investigated electrophiles, those able to follow a coupling process with MesMgBr display high first reduction potentials. Table 1 shows that the less negative the Ar'-X reduction potential, the higher the quantity of both cross-coupling and homocoupling products. For example, 2-chloro-5-trifluoromethylpyridine is easily reduced at -1.60 V vs SCE: since [Mes₃Fe^{II}]⁻ is the sole iron-containing species formed in the presence of an excess of MesMgBr, this suggests that 2-chloro-5-trifluoromethylpyridine might undergo a single-electron transfer (SET) activation by [Mes₃Fe^{II}]⁻, according to the path showed in Scheme 1a (cycle (i)). Moreover, when cross-coupling was performed between those two reagents in the presence of a radical quencher (TEMPO), only traces of coupling product were detected (Table 1, Entry 7), which also may indicate the involvement of a radical coupling sequence. Reactivity of [Mes₃Fe^{II}]⁻ towards 2-chloro-5-trifluoromethylpyridine has moreover been probed by ¹H NMR. Addition of 4 equiv. of 2-chloro-5-trifluoromethylpyridine onto [Mes₃Fe^{II}]⁻ led to the observation of [Mes₂Fe^{II}Br]⁻ as a minor species after 5 h at 20 °C, along with unreacted [Mes₃Fe^{II}]⁻ in a 30:70 ratio (see Figure S2; the signals of [Mes₂Fe^{II}Br]⁻ (δ = 131, 106 ppm) were attributed by comparison with a sample of [Mes₄Fe^{II}] treated by [nBu₄N⁺;Br⁻], see Figure S3); this ratio increased to a 75:25 value after 20 h (Figure 1a). Additionally to the formation of the dicoordinated complex [Mes₂Fe^{II}Br]⁻, ca. 10% of 2-mesityl-5-trifluoromethylpyridine were also detected by GC-MS (in line with the coupling yield given Table 1, Entry 7). [Mes₂Fe^{II}Br]⁻ can thus be obtained at the end of a coupling sequence between [Mes₃Fe^{II}]⁻ and 2-chloro-5-trifluoromethylpyridine, in which a mesityl group originally bound to the iron is coupled to the electrophile, leading to the formation of a formal dicoordinated intermediate Mes₂[Fe^{II}]. An anion metathesis with a bromine anion brought by MesMgBr finally affords [Mes₂Fe^{II}Br]⁻ which is detected by ¹H NMR.

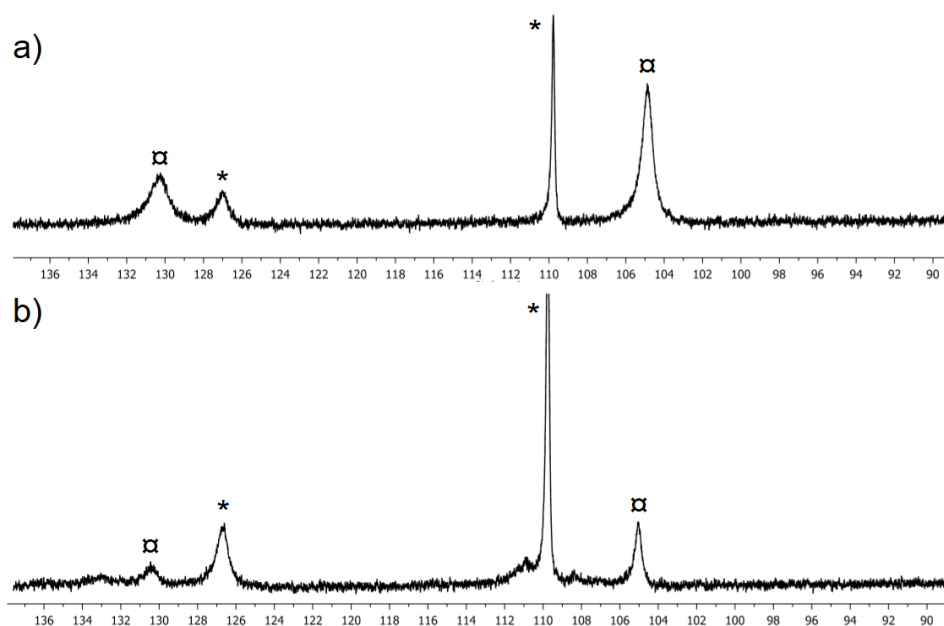


Figure 1: ^1H NMR spectra (60 MHz, 20 °C, THF d_8) of a solution of $[\text{Mes}_3\text{Fe}^{\text{II}}]^-$ (generated by addition of 5 equiv. MesMgBr onto $\text{Fe}(\text{acac})_3$) in the presence of 4 equiv. of a) 2-chloro-5-trifluoromethylpyridine; b) 2-chloropyrimidine, after 20 h at 20 °C; * = $[\text{Mes}_3\text{Fe}^{\text{II}}]^-$; α = $[\text{Mes}_2\text{Fe}^{\text{II}}\text{Br}]^-$. $\text{Fe}(\text{acac})_3$ was used as an iron source herein in order to limit the quantity of halide anions in the reaction medium which could favor the formation of dicoordinated $[\text{Mes}_2\text{Fe}^{\text{II}}\text{X}]^-$ species by anion metathesis.

For easily reduced heteroaryl halides (such as 2-chloro-5-trifluoromethylpyridine), this thus suggests that both cross-coupling and homocoupling cycles may be initiated by a one-electron $\text{Fe}^{\text{II}}/\text{Fe}^{\text{III}}$ sequence. Grignard homocoupling process may indeed also be enabled by a SET between an active organoiron(II) intermediate and an organic halide, since the oxidized Fe^{III} species obtained after the electron transfer is shared by both cross-coupling and homocoupling cycles ((i) and (ii) in Scheme 1a). 2-chloropyrimidine, 2-chloroquinoline and iodobenzene have more negative reduction potentials, lying between -1.9 and -2.0 V vs SCE (Entries 9, 11, 15). Accordingly, those substrates only afford small amounts of cross-coupling products with MesMgBr, along with traces of bisaryl MesMes. Furthermore, almost no coupling product was detected when the cross-coupling between MesMgBr and 2-chloropyrimidine was carried out in the presence of TEMPO (Table 1, Entry 9). This again suggests the occurrence of one-electron coupling processes, akin to what is observed using 2-chloro-5-trifluoromethylpyridine. The reactivity of $[\text{Mes}_3\text{Fe}^{\text{II}}]^-$ towards 2-chloropyrimidine has also been probed by ^1H NMR (Figure 1b). Treatment of the former by 4 equiv. of 2-chloropyrimidine leads to the

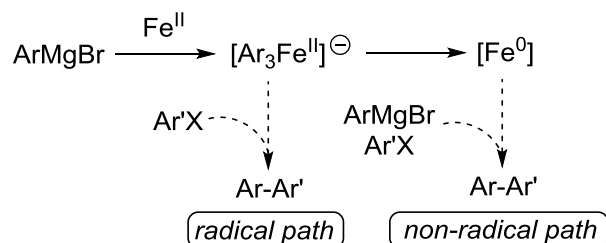
formation of a small quantity of $[\text{Mes}_2\text{Fe}^{\text{II}}\text{Br}]^-$ ($[\text{Mes}_2\text{Fe}^{\text{II}}\text{Br}]^-:[\text{Mes}_3\text{Fe}^{\text{II}}]^-$ ratio = 38:62) after 20 h at 20 °C, along with 3% of cross-coupling product detected by GC-MS. Those data reflect the relative reactivities of 2-chloropyrimidine and 2-chloro-5-trifluoromethylpyridine towards MesMgBr , the former being much less reactive than the latter (Table 1, Entries 9 and 7), and also support the reactivity of $[\text{Mes}_3\text{Fe}^{\text{II}}]^-$ as an on-cycle intermediate in cross-coupling processes involving easily reduced heteroaryl electrophiles.

The less activated 2-chloro-5-Z-pyridines (Z = H, F or Me, Entries 1, 3 and 5) as well as $\text{C}_6\text{F}_5\text{Cl}$ (Entry 13) are reduced at even more negative potentials, lower than -2.0 V vs SCE: for those substrates, no conversion is observed, and neither cross-coupling nor homocoupling products are obtained. This result is in line with the difficulty of carrying out a coupling process involving a single-electron transfer (SET) as the activation step when (hetero)aryl halides are used as electrophiles. The rate of the SET step is driven by the reduction potential of the C–Halide bond, which is itself related to the bond dissociation energy (BDE) of the latter: the less negative the reduction potential of the electrophile, the lower the BDE of the latter, and thus the faster the SET step.¹⁴

Taking into account those considerations, the absence of any trace of aryl-(hetero)aryl cross-coupling product using MesMgBr and (hetero)aryl electrophiles with very negative reduction potentials (that is, lower than -2 V vs SCE) can be seen as a token that the organoiron intermediates at the Fe^{II} oxidation state (e.g. $[\text{Mes}_3\text{Fe}^{\text{II}}]^-$) are not able to promote the aryl-heteroaryl coupling cycle when the latter relies on a SET activation of the electrophile. Therefore, it suggests that the coupling products (either cross-coupling or homocoupling) formed upon reaction of PhMgBr with electrophiles which remain unreactive in the presence of MesMgBr (Table 1, Entries 2, 4, 6, 14) are obtained during catalytic processes relying on iron oxidation states lower than +II, thus requiring *in-situ* generation of Fe^0 or Fe^{I} species (Scheme 1b). It is moreover noteworthy that the coupling sequence involving those low oxidation state species still operates in the presence of a radical quencher, since PhMgBr and 2-chloro-5-trifluoromethylpyridine afford 16 % of the coupling product in the presence of TEMPO (Table 1, Entry 8), whereas almost no coupling occurred with MesMgBr under the same conditions (*vide supra*). Radical-quenching experiments are thus consistent with the occurrence of two coupling regimes, the first one involving a Fe^{II} active species and a $\text{Fe}^{\text{II}}/\text{Fe}^{\text{III}}$ monoelectronic sequence, the second one relying on lower oxidation states involved in a non-radical route (Scheme 2). When PhMgBr is used as a nucleophile,

it is likely that cross-coupling products are formed independently by those two pathways, the *ate* $[\text{Ph}_3\text{Fe}^{\text{II}}]^-$ species being able to react prior to its reduction in an electron-transfer step with easily reduced electrophiles.

Scheme 2: two drastically different routes at work in aryl-(hetero)aryl Fe-mediated cross-couplings.



Stoichiometric and single-turnover experiments were monitored by paramagnetic ^1H NMR in order to shed light on the mechanism involved in the non-radical latter path, and to analyze the striking difference of behavior between mesityl- and phenyl-based couplings described in Table 1.

When $[\text{Mes}_3\text{Fe}^{\text{II}}]^-$ (generated by addition of 4 equiv. MesMgBr onto FeCl_2 , see Figure S1) was treated by an excess (10, 70, or 140 equiv.) of 2-PyCl, ^1H NMR monitoring showed the former as the sole species in the 20-150 ppm area. No evolution of $[\text{Mes}_3\text{Fe}^{\text{II}}]^-$ signals was observed after 20 h at 20 °C, attesting to the absence of reaction with the heteroaryl halide (see Figure S4), in agreement with the absence of coupling reactivity reported for this set of reagents (Table 1, Entry 1). Moreover, since dicoordinated mesityliron(II) intermediates such as $[\text{Mes}_2\text{Fe}^{\text{II}}\text{Br}]^-$ can coexist with $[\text{Mes}_3\text{Fe}^{\text{II}}]^-$ in THF solutions,¹¹ the reactivity of a mixture of those two species formed by action of $[\text{nBu}_4\text{N}^+;\text{Br}^-]$ onto the dinuclear complex $[\text{Mes}_4\text{Fe}_2^{\text{II}}]$ has also been investigated. No evolution of the ^1H NMR signals of $[\text{Mes}_2\text{Fe}^{\text{II}}\text{Br}]^-$ and $[\text{Mes}_3\text{Fe}^{\text{II}}]^-$ has been observed upon addition of a large quantity of 2-PyCl (up to 70 equiv., see Figure 2a).¹⁵

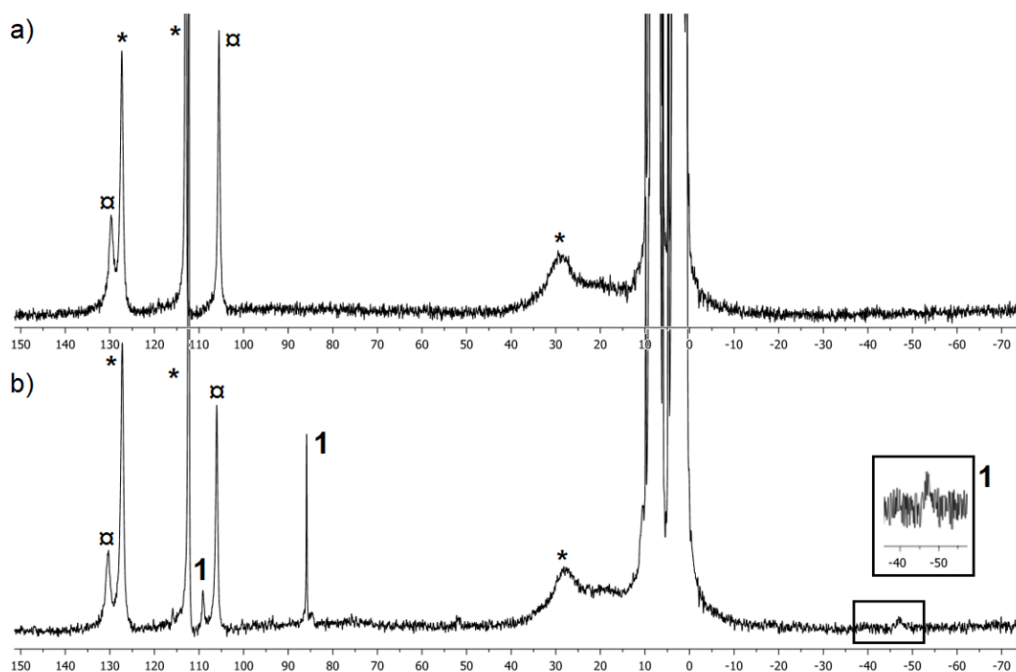


Figure 2: ¹H NMR spectra (60 MHz, 20 °C, THF *d*₈) of a) a 40:60 distribution of [Mes₂Fe^{II}Br]⁻ and [Mes₃Fe^{II}]⁻ (generated by addition of 10 equiv. [*n*Bu₄N⁺;Br⁻] onto [Mes₄Fe₂^{II}]) treated by 70 equiv. 2-PyCl at 20 °C during 4 h; and b) of a solution of [Mes₃Fe^{II}]⁻ (generated by addition of 4 equiv. MesMgBr onto FeCl₂) in the presence of an excess of 2-PyCl (70 equiv.), after addition of PhMgBr (2 equiv.); * = [Mes₃Fe^{II}]⁻; □ = [Mes₂Fe^{II}Br]⁻.

In both cases, no traces of 2-mesitylpyridine were detected by GC-MS analysis, in agreement with the results discussed in the previous section (Table 1, Entry 1). In other words, this demonstrates that neither the homoleptic species [Mes₃Fe^{II}]⁻ nor its dicoordinated analogue [Mes₂Fe^{II}Br]⁻ are able to initiate an aryl-heteroaryl coupling cycle, strengthening the hypothesis that formation of oxidation states lower than Fe^{II} is required to enter the catalytic process (Scheme 3a).

obtained upon treatment of $[\text{Mes}_3\text{Fe}^{\text{II}}]^-$ by 2-PyMgBr in the presence of 2-PyCl (see Figure S5). Those results show that treatment of $[\text{Mes}_3\text{Fe}^{\text{II}}]^-$ by PhMgBr in the presence of 2-PyCl leads to the formation of species $[\text{Mes}_2(2\text{-Py})\text{Fe}^{\text{II}}]^-$, thus featuring a formal 2-Py⁻ anion. No trace of chlorobenzene was detected under those conditions or in the absence of iron, thus ruling out the formation of such pyridyl anions by halogen-metal exchange between the Grignard and the starting 2-chloro-5-Z-pyridine (Z = H or CF₃). In other words, those conditions enable the activation of the C—Cl bond of 2-PyCl by a two-electron reduction process. Importantly, this suggests that addition of PhMgBr first led to *in situ* two-electron reduction of $[\text{Mes}_3\text{Fe}^{\text{II}}]^-$ at the Fe⁰ stage, and that the latter Fe⁰ species reacted with 2-PyCl to afford a transient (2-Py)—[Fe^{II}] intermediate ultimately trapped as an *ate*-iron(II) high-spin complex $[\text{Mes}_2(2\text{-Py})\text{Fe}^{\text{II}}]^-$ (**1**) by reaction with the excess of MesMgBr (Scheme 3b, with Ar' = 2-Py).

A similar result was obtained using C₆F₅Cl as electrophile: reduction of $[\text{Mes}_3\text{Fe}^{\text{II}}]^-$ by PhMgBr in the presence of 70 equiv. C₆F₅Cl led to the observation of a new downfielded paramagnetic species in ¹H NMR (δ = 136 and 156 ppm, Figure 3a), diagnostic of a high-spin Fe^{II}-ligated mesityl ligand. Accordingly, ¹⁹F NMR also showed two highly downfielded paramagnetic signals at 202 and 300 ppm (Figure 3b). Those data also attest that C₆F₅Cl was turned into an anionic ligand σ-bonded to a high-spin Fe^{II} center. This therefore also suggests a two-electron reduction of C₆F₅Cl at the C₆F₅⁻ stage by an *in-situ* generated Fe⁰ species (Scheme 3b, Ar' = C₆F₅), followed by a nucleophilic trapping by MesMgBr leading to the formation of $[\text{Mes}_2(\text{C}_6\text{F}_5)\text{Fe}^{\text{II}}]^-$ (**2**). Formation of a two-electron reduced product of C₆F₅Cl under those conditions was also confirmed by treating separately $[\text{Mes}_3\text{Fe}^{\text{II}}]^-$ with 2 equiv. C₆F₅MgBr, which led to the formation of the same paramagnetic species (Figure 3c).

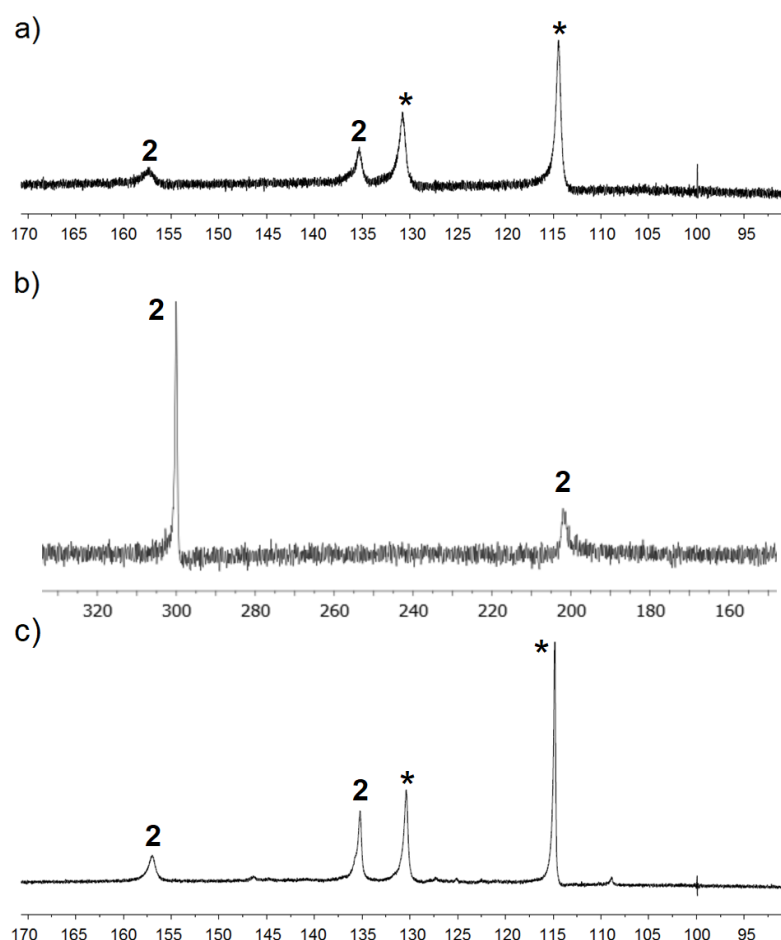


Figure 3: a) ^1H NMR (60 MHz, 20 °C, THF d_8) and b) ^{19}F NMR (377 MHz, THF d_8) spectra of a solution of $[\text{Mes}_3\text{Fe}^{\text{II}}]^-$ treated by 2 equiv. PhMgBr in the presence of 70 equiv. $\text{C}_6\text{F}_5\text{Cl}$; c) ^1H NMR spectrum of a solution of $[\text{Mes}_3\text{Fe}^{\text{II}}]^-$ treated by 2 equiv. $\text{C}_6\text{F}_5\text{MgBr}$; * = $[\text{Mes}_3\text{Fe}^{\text{II}}]^-$.

Detection of $[\text{Mes}_2(\text{Ar}')\text{Fe}^{\text{II}}]^-$ species ($\text{Ar}' = 2\text{-Py}$ or C_6F_5) starting from a Fe^0 complex generated *in situ* in the presence of the corresponding (hetero)aryl chlorides shows that a two-electron process involving the $\text{Fe}^0 / \text{Fe}^{\text{II}}$ couple can be at play in the activation of the $\text{Ar}'\text{-Cl}$ bond. The absence of detection of bisaryls $\text{Ar}'\text{-Ar}'$ formed by one-electron reduction of an organic halide $\text{Ar}'\text{-Cl}$ followed by radical recombination may also suggest that this transformation involving the $\text{Fe}^0 / \text{Fe}^{\text{II}}$ couple is a genuine one-step concerted two-electron process, which does not involve two successive one-electron elementary steps. Activation of an organic halide by successive SETs indeed leads to homocoupling of the latter. Overall two-electron oxidative addition of

benzyl bromide onto an iron(0) complex involving a $\text{Fe}^0 / \text{Fe}^{\text{I}} / \text{Fe}^{\text{II}}$ sequence was described by Sen using the anionic complex $[\text{CpFe}^0(\text{cod})][\text{Li}(\text{tmeda})]$ (Scheme 3c).^{18a} In those conditions, complex $(\text{tmeda})\text{Fe}^{\text{II}}(\text{CH}_2\text{Ph})_2$ is obtained, and reacts with an excess of benzyl bromide in a radical pathway to afford homocoupling product $\text{Ph}(\text{CH}_2)_2\text{Ph}$. Prevalence of a SET-based mechanism in the latter case seems to originate from the high reduction potential of PhCH_2Br ($-1.68 \text{ V vs SCE}^{18b}$), which leads to the easy generation of the benzyl radical $\text{PhCH}_2\cdot$. A similar two-step oxidative addition with successive SETs was also suggested by Cahiez for Kochi-Kumada aryl-alkyl cross-couplings, albeit without experimental support.^{18c} Therefore, the results detailed earlier in this section support the occurrence of a one-step two-electron oxidative addition process which can connect a Fe^0 complex with a well-defined organoiron(II) intermediate. Kinetics data were gathered in a second time in order to outline the mechanistic pattern of this process.

The kinetic law of the coupling involving PhMgBr and 2-PyCl (Table 1, Entry 2) has been determined using the method of the initial rates (Figure 4). The couplings were carried out at 0°C using either FeCl_2 or FeCl_3 salts as iron precursors, and the formation of the coupling product 2-PyPh was monitored by GC-MS analysis (see Figures S6-8). Similar results were obtained regardless of the nature of the precursor.

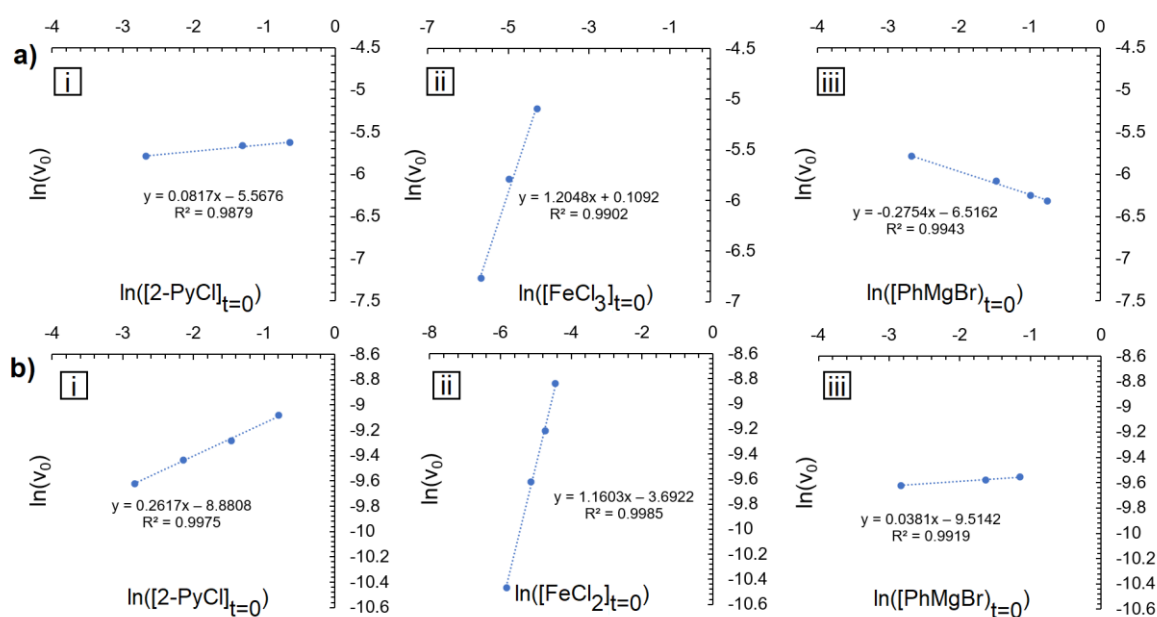


Figure 4: influence of the starting concentration of 2-PyCl (i), FeCl_n (ii) and PhMgBr (iii) on the initial cross-coupling rate of 2-PyCl and PhMgBr at 0 °C, mediated by a) FeCl₃ and b) FeCl₂. The slope of the ln / ln plot in each case is the order of the corresponding reagent in the kinetics rate law.

The global kinetics fit with a zeroth order in both 2-PyCl and PhMgBr, and a first order in iron (n = 2 or 3):

$$v = k.[2\text{-PyCl}]^0.[\text{FeCl}_n]^1.[\text{PhMgBr}]^0 = k.[\text{FeCl}_n]$$

The similar kinetics followed by the system regardless of the nature of the starting precursor reveal that reduction of the latter towards the active Fe⁰ species is not the rate-determining step. This is in agreement with recent reports showing that reduction of ferrous and ferric chloride salts by unhindered aryl Grignard reagents quickly proceeds at those temperatures.^{6b,19} The zeroth order in PhMgBr also clearly shows that no transmetallation towards either the catalytically active oxidation state or towards the Fe^{II/III} precursors is involved in the rate-determining step. This behavior strongly differs from that described by Hu for aryl-alkyl cross-coupling mediated by a bis(oxazolinyphenyl)amido (Bopa) iron(II) complex. In that system, a first order in nucleophile and a second order in iron suggested that transmetallation of an aryl group proceeding within a bimetallic intermediate was the rate-determining step²⁰

It also appears that the overall coupling process is much faster when FeCl₃ is used as a precursor. Extraction of the ordinate at origin from curves given in Figures 4-a-ii and b-ii indeed gives a much higher rate constant when starting from FeCl₃ precursor than from FeCl₂ :

$$\ln(k_{\text{FeCl}_3}/k_{\text{FeCl}_2}) = 2.45,$$

thus meaning that the coupling rate constant is ca. 12 more times higher in the former case. This difference of behavior between those two precursors likely originates in the lack of solubility of FeCl₂ in THF at 0 °C. Unlike FeCl₃ which is fully soluble in those conditions, FeCl₂ indeed leads to a barely soluble polynuclear

$[\text{Fe}_4\text{Cl}_8(\text{THF})_6]$ species in THF.²¹ Destruction of the latter structure by the action of PhMgBr prior to reduction of the Fe^{II} species at the Fe^0 stage thus requires an additional energetic barrier. This is mirrored by the relative Grignard rate orders in the kinetics laws: orders extracted from Figures 4-a-iii and b-iii are close to zero, but the PhMgBr order obtained starting from FeCl_2 is slightly higher, attesting to the benefic role of PhMgBr in the solubilization of polynuclear $[\text{Fe}_4\text{Cl}_8(\text{THF})_6]$ prior to its reduction. Conversely, the slightly negative order obtained for PhMgBr when starting from FeCl_3 might attest to the easier reduction of the latter towards non-reactive iron particles in the presence of an excess of PhMgBr.

The coupling moreover proceeds with increased rates when electron-deficient electrophiles are employed. Kinetics analysis was performed on a series of 5-substituted 2-chloropyridines used as electrophiles along with PhMgBr, and a linear Hammett plot has been obtained, displaying a positive slope ($\rho = 2.76$, Figure 5).

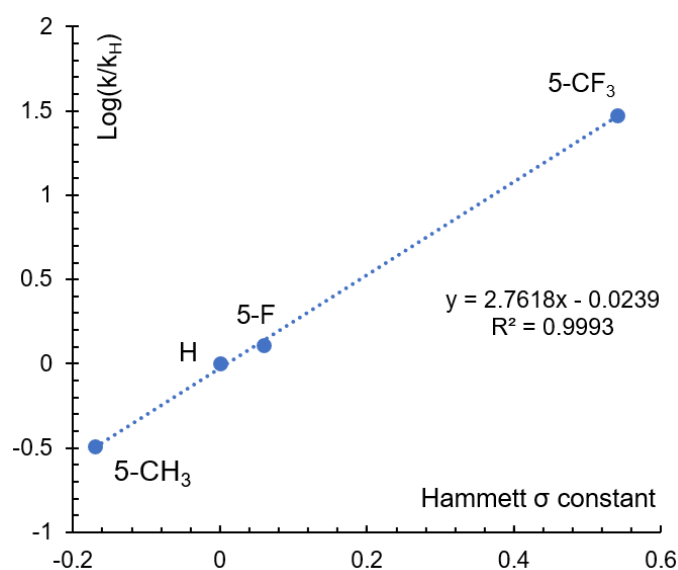


Figure 5: Hammett plot obtained for the cross-coupling between PhMgBr and 5-substituted 2-chloropyridines; conditions: FeCl_2 10 mol%, THF, 0°C .

Aiming at obtaining a mechanistic picture mirroring those experimental kinetics tendencies, the elementary steps at play in the two-electron coupling mechanism between 2-chloropyridine and an aryl Grignard reagent ArMgX were then investigated *in silico* by means of DFT calculations. A particular focus was put on delineating the pathway leading to the experimentally observed species $[\text{Ar}_2(\text{Ar}')\text{Fe}^{\text{II}}]^-$ ($\text{Ar}' = 2\text{-Py}$ and C_6F_5 ,

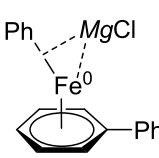
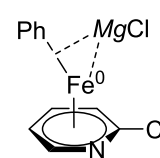
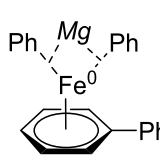
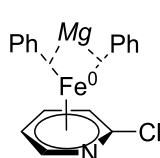
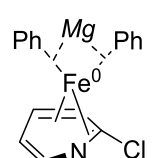
Figures 2 and 3), as well as the role of the latter in the coupling process itself. PhMgCl and 2-chloropyridine were chosen as models for the coupling reagents. We made the choice to limit this theoretical work to the reactivity of well-defined organometallic species containing a sole iron center. Therefore, due to the complexity of such “ligand-free” coupling systems which can sometimes lead to the formation of multinuclear intermediates under catalytically-relevant conditions,^{3c} the results discussed in the next section provide a qualitative, simplified picture of the real system. This computational work was carried out using the Gaussian09 code,^{22a} and OPBE functional was chosen, since it proved to efficiently reproduce both electronic and thermic properties of iron complexes, regardless of their oxidation and spin states.^{22b-d} Implicit PCM solvation model^{22e,f} was associated with explicit solvation of the magnesium adducts by THF molecules (see SI).

The first step of the DFT analysis was to decipher the nature of the organometallic resting state obtained after reduction of the iron precursor at the bis-arene-Fe⁰ stage (Scheme 1b). In the absence of toluene, biphenyl PhPh formed upon reduction by PhMgBr can also act as a stabilizing ligand, as demonstrated by Hu for the biphenyl-ligated *ate*-Fe^I complex $[(\eta^6\text{-PhPh})\text{Fe}^{\text{I}}(\text{Ph})_2]^-$,²³ analogue of the η^6 -toluene complex displayed in Scheme 1b. The fate of the complex Fe⁰(PhPh)₂ in catalytically-relevant conditions, that is, in the presence of 2-PyCl and of an aryl Grignard reagent, has thus been investigated. Ligand substitution at Fe⁰ can occur since 2-PyCl also acts as a neutral η^n ligand ($n = 2, 4$ or 6) such as PhPh. Moreover, phenyl anions Ph⁻ brought by the Grignard can also act as a strong anionic σ -coordinating ligand to the Fe⁰.²⁴ The relative free energies of the bis-arene coordinated complexes $(\eta^{4/6}\text{-PhPh})_2\text{Fe}^0$, $(\eta^6\text{-PhPh})(\eta^4\text{-2-PyCl})\text{Fe}^0$ and $(\eta^{4/6}\text{-2-PyCl})_2\text{Fe}^0$, as well as that of the mono-transmetallated $(\eta^6\text{-PhPh})\text{Fe}^0(\text{PhMgCl}\cdot\text{THF})$ (**A-Fe⁰_{PhPh,Ph}**), $(\eta^6\text{-2-PyCl})\text{Fe}^0(\text{PhMgCl}\cdot\text{THF})$ (**A-Fe⁰_{PyCl,Ph}**), and double-transmetallated species $(\eta^6\text{-PhPh})\text{Fe}^0(\text{PhMgPh}\cdot\text{THF})$ (**B-Fe⁰_{PhPh,2Ph}**), $(\eta^4\text{-2-PyCl})\text{Fe}^0(\text{PhMgPh}\cdot\text{THF})$ (**B-Fe⁰_{PyCl,2Ph}**), are given in Table 2. All species have been computed at singlet ($S = 0$) and triplet ($S = 1$) states, except **B-Fe⁰_{PhPh,2Ph}**, for which no stable bis-arylliron(0) structure has been found at the triplet state (a migration of a phenyl anion onto the Mg^{II} cation being observed). Bis-arene ligated complexes (columns 1-3 in Table 2) are formally 18-electron species, the arene ligands playing unsymmetrical roles (one adopting a η^6 coordination mode, the second a η^4 coordination). Those results suggest that progressive substitution of the PhPh ligands in Fe⁰(PhPh)₂ by 2-PyCl leads to a

slight destabilization of the coordination sphere ($0.3 \text{ kcal.mol}^{-1}$ for the first substitution, $5.5 \text{ kcal.mol}^{-1}$ for the second one, see Table 2). Moreover, for all those bis-arene ligated species, the triplet state ($S = 1$) was found to be more stable than the singlet ($S = 0$).

Table 2. DFT-computed thermal free energies formation (G_{th}) of plausible Fe^0 species ligated by 2-PyCl or PhMgCl starting from $^3(\eta^6\text{-PhPh})_2Fe^0$. PhMgCl•(THF)₂ has been taken as a solvated model for PhMgCl. Theory level : OPBE, 6-31+G*, def2TZVPP and pseudo-potential (Fe); PCM (THF); $Mg = Mg(THF)^{2+}$.

		$(\eta^{4/6}\text{-PhPh})_2Fe^0$	$(\eta^6\text{-PhPh})(\eta^4\text{-2-PyCl})Fe^0$	$(\eta^{4/6}\text{-2-PyCl})_2Fe^0$
$S = 0$	G_{th}	4.0	5.5	13.8
$S = 1$	G_{th}	0.0	0.3	5.5

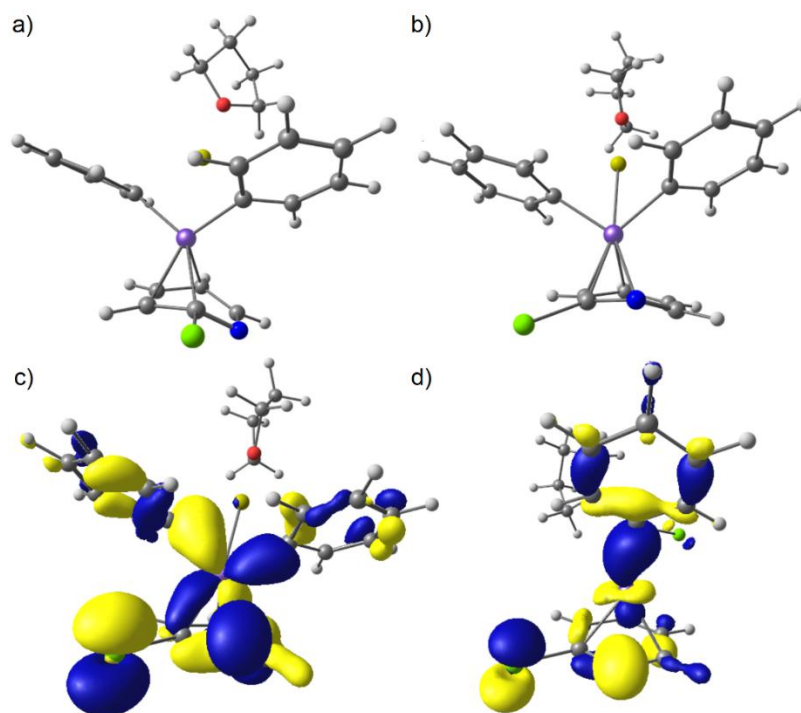
		$(\eta^6\text{-L})Fe^0(\text{PhMgCl}\cdot\text{THF})$		$(\eta^{4/6}\text{-L})Fe^0(\text{Ph}_2\text{Mg}\cdot\text{THF})$		
						
		A-Fe⁰_{PhPh,Ph}	A-Fe⁰_{PyCl,Ph}	B-Fe⁰_{PhPh,2Ph}	B-Fe⁰_{PyCl,2Ph}	C-Fe⁰_{PyCl,2Ph}
		L = PhPh	L = 2-PyCl	L = PhPh	L = 2-PyCl	L = 2-PyCl
$S = 0$	G_{th}	-3.2	2.5	-9.4	-9.9	-
$S = 1$	G_{th}	-16.4	-13.4	-	-5.8	0.7

As outlined in Table 2, substitution of a PhPh ligand in $(\text{PhPh})_2Fe^0$ by one Ph^- anion leads to complex **A-Fe⁰_{PhPh,Ph}**, with a strong stabilization by ca. 16.4 kcal.mol⁻¹. Second coordination by Ph^- affords complex **B-Fe⁰_{PhPh,2Ph}**, stabilized by 9.4 kcal.mol⁻¹ with respect to $(\text{PhPh})_2Fe^0$. The ground states of the 2-PyCl-ligated analogues of the latter complexes, **A-Fe⁰_{PyCl,Ph}** and **B-Fe⁰_{PyCl,2Ph}**, have been respectively located at -13.4 and -9.9 kcal.mol⁻¹, suggesting a possible equilibrium within this distribution of Fe^0 complexes. It is noteworthy that the monoaryl complexes **A-Fe⁰_{PhPh,Ph}** and **A-Fe⁰_{PyCl,Ph}** display a strong preference for a high-spin ground state ($S = 1$; $G_{S=1} - G_{S=0} = -15.9$ kcal.mol⁻¹ for the latter), whereas the bis-aryl analogues **B-Fe⁰_{PhPh,2Ph}** and **B-Fe⁰_{PyCl,2Ph}** accommodate a low-spin configuration ($S = 0$; $G_{S=1} - G_{S=0} = 4.1$ kcal.mol⁻¹ for the latter). Similar respective preferences for high-spin ($S = 3/2$) and low-spin ($S = 1/2$) configurations were also evidenced by some of us *in silico* for analogous mono- and bis-aryl arene-coordinated organoiron(I) species, in agreement

with experimental data.²⁵ ${}^3\mathbf{A}\text{-Fe}^0_{\text{PhPh,Ph}}$ is thus predicted to be the most stable Fe^0 resting state obtained in the presence of 2-PyCl and PhMgCl, and is in equilibrium with 2-PyCl-coordinated complexes ${}^3\mathbf{A}\text{-Fe}^0_{\text{PyCl,Ph}}$ and ${}^1\mathbf{B}\text{-Fe}^0_{\text{PyCl,2Ph}}$, respectively stabilized by one and two σ -bonded Ph^- ligands. In other words, this means that PhPh can stabilize transiently the Fe^0 oxidation state prior to coordination of the 2-chloropyridine onto the metal. It cannot be excluded that adducts with a higher Mg:Fe ratio are also involved (that is, species involving chelation by more than one equiv. of PhMgX or PhMgPh per mole of iron); such adducts have not been included in the present simplified analysis.

Amongst the distribution of 2-PyCl-ligated Fe^0 species (that is : ${}^3\mathbf{A}\text{-Fe}^0_{\text{PyCl,Ph}}$, ${}^1\mathbf{A}\text{-Fe}^0_{\text{PyCl,Ph}}$, ${}^3\mathbf{B}\text{-Fe}^0_{\text{PyCl,2Ph}}$ and ${}^1\mathbf{B}\text{-Fe}^0_{\text{PyCl,2Ph}}$), the case of ${}^3\mathbf{B}\text{-Fe}^0_{\text{PyCl,2Ph}}$ is particularly interesting due to the flexibility of the η^4 -coordination modes of the 2-PyCl ligand. The ground state of ${}^3\mathbf{B}\text{-Fe}^0_{\text{PyCl,2Ph}}$ features a $\eta^4\text{-(C}_2\text{C}_3\text{C}_4\text{C}_5\text{)}$ coordination of the 2-PyCl ligand (Scheme 4a). The latter can undergo an hapticity shift, adopting a $\eta^4\text{-(NC}_2\text{C}_3\text{C}_4\text{)}$ coordination and leading to complex ${}^3\mathbf{C}\text{-Fe}^0_{\text{PyCl,2Ph}}$ (Table 2 and Scheme 4b), located $6.5 \text{ kcal.mol}^{-1}$ above the former (overall $17.1 \text{ kcal.mol}^{-1}$ free energy formation from ${}^3\mathbf{A}\text{-Fe}^0_{\text{PhPh,Ph}}$). Importantly, this hapticity shift also precludes the formation of a stronger Fe-C_2 bond, akin to what occurs upon formation of a Meisenheimer adduct. The Fe-C_2 bond indeed becomes shorter in ${}^3\mathbf{C}\text{-Fe}^0_{\text{PyCl,2Ph}}$ (1.93 \AA versus 2.03 \AA in ${}^3\mathbf{B}\text{-Fe}^0_{\text{PyCl,2Ph}}$), and a deviation of the $\text{C}_2\text{-Cl}$ bond outside of the medium $\text{NC}_2\text{C}_3\text{C}_4$ plan is observed, *anti* to the Fe-C_2 bond ($\angle(\text{FeC}_2\text{Cl}) = 130.6^\circ$ in ${}^3\mathbf{C}\text{-Fe}^0_{\text{PyCl,2Ph}}$ versus 126.4° in ${}^3\mathbf{B}\text{-Fe}^0_{\text{PyCl,2Ph}}$).

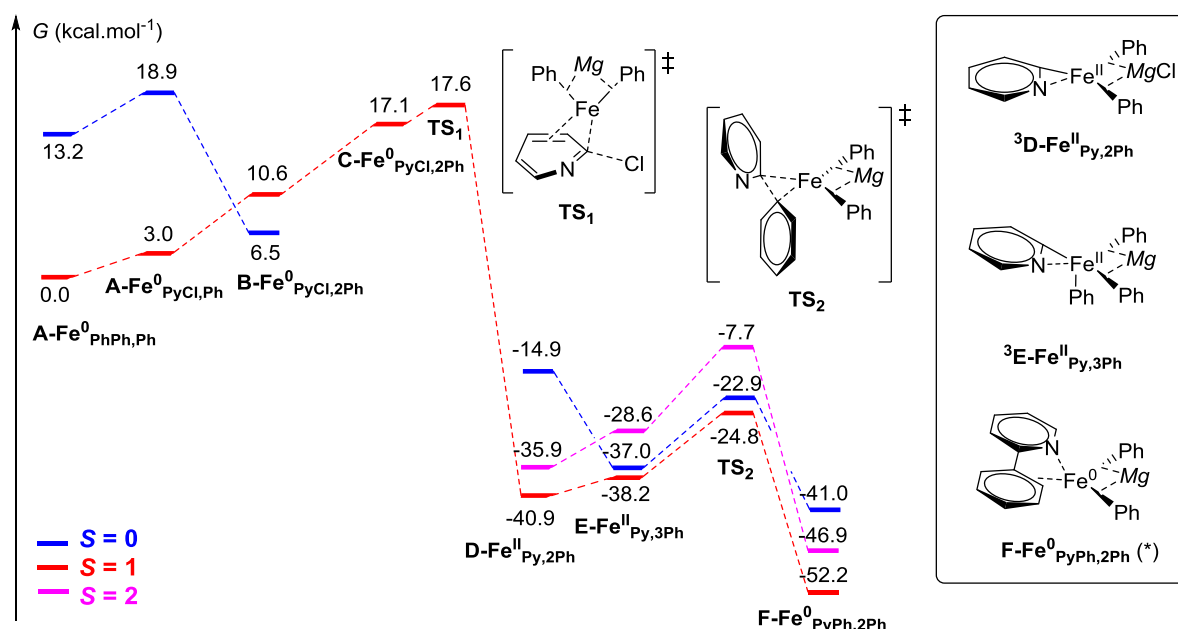
Scheme 4: DFT computed structures of a) ${}^3\mathbf{B}\text{-Fe}^0_{\text{PyCl}_2\text{Ph}}$ and b) ${}^3\mathbf{C}\text{-Fe}^0_{\text{PyCl}_2\text{Ph}}$; molecular orbitals featuring bonding interactions between Ph^- ligands and Fe^0 center in c) ${}^3\mathbf{C}\text{-Fe}^0_{\text{PyCl}_2\text{Ph}}$ ($\alpha_{\text{HOMO-11}}$) and d) ${}^3\mathbf{A}\text{-Fe}^0_{\text{PyCl}_2\text{Ph}}$ ($\alpha_{\text{HOMO-11}}$).



Adduct ${}^3\mathbf{C}\text{-Fe}^0_{\text{PyCl}_2\text{Ph}}$ thus can be seen as a pre-complex on the way to the activation of the $\text{C}_2\text{—Cl}$ bond by an intramolecular oxidative addition in a $\text{S}_{\text{N}}\text{Ar}$ -like mechanism. A similar bis-phenyl adduct featuring an ongoing formation of the Fe—C_2 bond could not be located on the singlet surface ($S = 0$), nor could be a similar mono-phenylated intermediate starting from the mono-aryl triplet complex ${}^3\mathbf{A}\text{-Fe}^0_{\text{PyCl}_2\text{Ph}}$. This can be a consequence of the symmetry of the molecular orbitals describing the Ph—Fe^0 bonds in those complexes. In complex ${}^3\mathbf{C}\text{-Fe}^0_{\text{PyCl}_2\text{Ph}}$, the bonding molecular orbital between the two aryl anions σ -ligated to the Fe^0 and the latter has a favorable d_{yz} symmetry allowing a positive overlap with the $\pi^*(\text{C}_2\text{—Cl})$ orbital (Scheme 4c), making possible the creation of a Fe—C_2 bond for symmetry reasons. On the other hand, the coordination of a single aryl group to the Fe^0 in ${}^3\mathbf{A}\text{-Fe}^0_{\text{PyCl}_2\text{Ph}}$ leads to a bonding $\text{Fe}^0\text{—Ph}$ molecular orbital with a d_{z^2} symmetry (Scheme 4d), making the overlap with the $\pi^*(\text{C}_2\text{—Cl})$ orbital unfavorable, thus hampering an efficient formation of a Fe—C_2 bond. ${}^3\mathbf{C}\text{-Fe}^0_{\text{PyCl}_2\text{Ph}}$ evolves following transition state ${}^3\mathbf{TS}_1$ (Scheme 5) to afford the heteroleptic *ate* complex

$^3[\text{Ph}_2(2\text{-Py})\text{Fe}^{\text{II}}\cdot\text{MgCl}(\text{THF})]$ ($^3\text{D-Fe}^{\text{II}}_{\text{Py},2\text{Ph}}$) with a small $0.5 \text{ kcal}\cdot\text{mol}^{-1}$ computed activation barrier. $^3\text{TS}_1$ enables the progressive breaking of the $\text{C}_2\text{—Cl}$ bond and the creation of a covalent Fe—C_2 bond ($d(\text{Fe—C}_2) = 1.89 \text{ \AA}$ in $^3\text{TS}_1$). $^3\text{D-Fe}^{\text{II}}_{\text{Py},2\text{Ph}}$ is obtained in an overall exothermic step (stabilization of $40.9 \text{ kcal}\cdot\text{mol}^{-1}$ with respect to the reactants, Scheme 5).

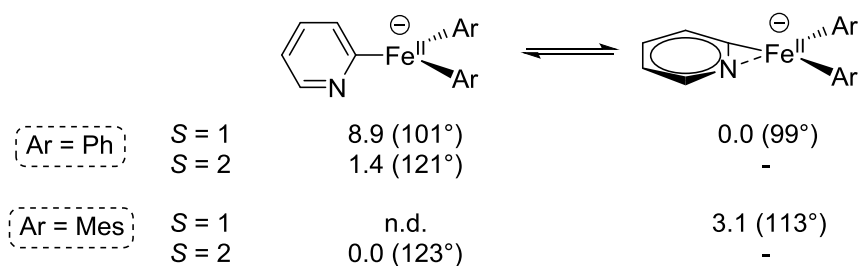
Scheme 5: DFT-computed surface for the cross-coupling between PhMgCl and 2-PyCl , starting from the Fe^0 resting state $^3\text{A-Fe}^0_{\text{PhPh,Ph}}$ (for clarity, free energies are given with respect to the latter); (*) : ground quintet state features a high-spin Fe^{I} center ($S = 3/2$) with an unpaired electron delocalized on the 2-PhPy ligand ($S = 1/2$).



In solution, complex $^3\text{D-Fe}^{\text{II}}_{\text{Py},2\text{Ph}}$ can afford the free anion $[\text{Ph}_2(2\text{-Py})\text{Fe}^{\text{II}}]^-$, which corresponds to the usually observed form of such tris-coordinated aryliron(II) complexes.^{ii,6c} Although tris-coordinated $[\text{Ar}_3\text{Fe}^{\text{II}}]^-$ species ($\text{Ar} = \text{Mes}, \text{Ph}, \dots$) usually feature a high-spin ($S = 2$) iron(II) ion, DFT optimization suggests that a greater stability is acquired by $[\text{Ph}_2(2\text{-Py})\text{Fe}^{\text{II}}]^-$ in the triplet state ($S = 1$, Scheme 5). The latter can indeed involve a ligation of the metal by the nitrogen atom of the pyridyl ring, leading to a more stable pseudo square-planar tetra-coordinated triplet isomer (Scheme 6, stabilization by $8.9 \text{ kcal}\cdot\text{mol}^{-1}$ with respect to the tris-coordinated less stable triplet isomer). Due to the presence of electrons in all d orbitals of the high-spin ($S = 2$) state, such

a ligation cannot occur for the high-spin isomer $^5[\text{Ph}_2(2\text{-Py})\text{Fe}^{\text{II}}]^-$, located $1.4 \text{ kcal.mol}^{-1}$ higher. Those results should of course be compared to experimental analysis of the corresponding species, but they at least suggest that spin interconversion in *ate*-iron(II) complexes might be easier for those bearing ligands with chelating atoms in the 2-position. On the other hand, DFT modelling of the bulkier mesityl analogue $[\text{Mes}_2(2\text{-Py})\text{Fe}^{\text{II}}]^-$ shows a pronounced preference for a tris-coordinated geometry, with no ligation of the nitrogen atom of the 2-pyridyl ring onto the Fe^{II} ion. A high-spin state ($S = 2$) is thus preferred in that case to the triplet, tetra-coordinated isomer, by ca. 3 kcal.mol^{-1} . This is in agreement with the ^1H NMR detection of species **1** (Figure 2) in the classic high-spin iron(II) area for such compounds.

Scheme 6: variety of coordination of the 2-pyridyl ligand in $[\text{Ar}_2(2\text{-Py})\text{Fe}^{\text{II}}]^-$ complexes (Ar = Ph, Mes) depending on their spin multiplicity. Relative computed free energies are reported in kcal.mol^{-1} ; Ar–Fe–Ar angle is given between parentheses.



The discrepancy between $[\text{Ph}_2(2\text{-Py})\text{Fe}^{\text{II}}]^-$ and $[\text{Mes}_2(2\text{-Py})\text{Fe}^{\text{II}}]^-$ (ground tetra-coordinated triplet state for the former, tris-coordinated quintet state for the latter) mostly originates in the difference of steric pressure brought by the Ph and Mes groups. Evolution of the Fe^{II} coordination sphere of complex $[\text{Ar}_2(2\text{-Py})\text{Fe}^{\text{II}}]^-$ from a trigonal environment to a pseudo-square planar geometry offers an electronic stabilization for the low spin multiplicities (herein $S = 1$). However, this evolution requires a drastic diminution of the Ar–Fe–Ar angle (see Scheme 6). For Ar groups bearing bulky substituents in the position *ortho* to the iron ion, this evolution also leads to an increase of the steric pressure. Thus, in the case of complex $[\text{Ph}_2(2\text{-Py})\text{Fe}^{\text{II}}]^-$, no steric factor counterbalances the energetic gain offered by the pseudo square-planar geometry, whereas the sterically

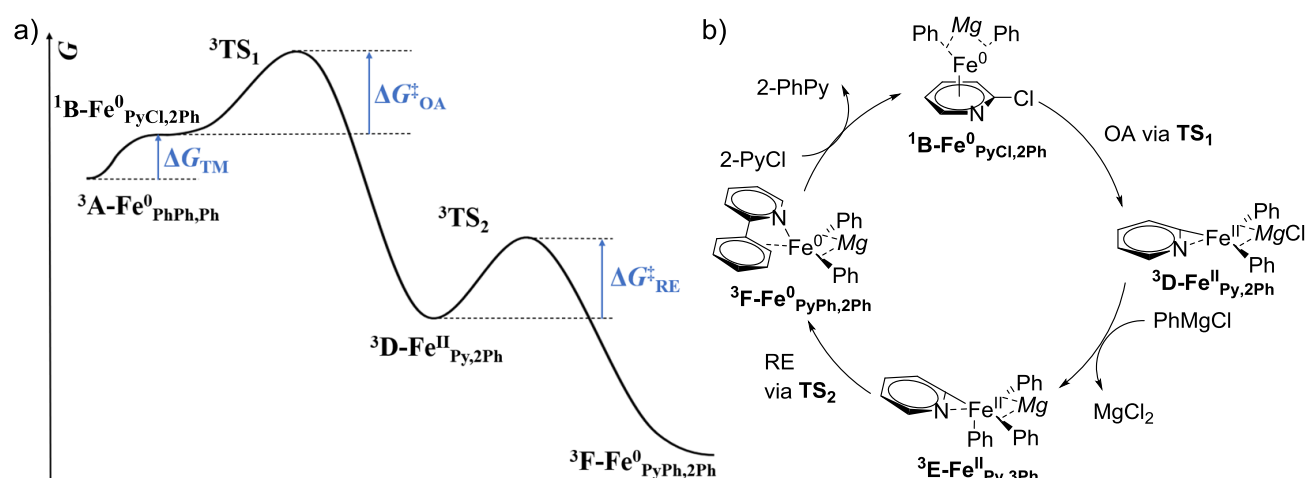
demanding mesityl groups in $[\text{Mes}_2(2\text{-Py})\text{Fe}^{\text{II}}]^-$ strongly compensate this electronic gain, making more favored the tris-coordinated isomer (and, therefore, the high-spin configuration usually observed in this case). Similar antagonist steric and electronic effects and their implications on the ground spin states and geometries of tetracoordinated $\text{Mes}_2\text{Fe}^{\text{II}}\text{L}_2$ species (L = phosphine, amine) were also reported by Chirik in the past (see reference in note 16).

The last step of the coupling process, that is, the formation of 2-phenylpyridine, occurs by elimination of the Ph–Py bond at the Fe^{II} ion. Reductive elimination of a bis-aryl product from a *tris*-arylrone(II) intermediate can be enhanced by a quaternization of the Fe^{II} ion involving an additional equivalent of nucleophile. We indeed showed recently that reductive elimination of Ph–Ph from the quaternized adduct $[\text{Ph}_4\text{Fe}^{\text{II}}\text{MgBr}(\text{THF})]^-$ could proceed with a $13.0 \text{ kcal.mol}^{-1}$ computed barrier, which is lower by $3.0 \text{ kcal.mol}^{-1}$ than that of *tris*-coordinated analogue $[\text{Ph}_3\text{Fe}^{\text{II}}]^-$.^{6c} Quaternization of ${}^3\text{D-Fe}^{\text{II}}_{\text{Py},2\text{Ph}}$ proceeds with a small $2.7 \text{ kcal.mol}^{-1}$ endergonicity, leading to ${}^3\text{E-Fe}^{\text{II}}_{\text{Py},3\text{Ph}}$ (Scheme 5). Reductive elimination of 2-PhPy from quaternized adduct ${}^3\text{E-Fe}^{\text{II}}_{\text{Py},3\text{Ph}}$ can then proceed on the triplet surface with a $13.4 \text{ kcal.mol}^{-1}$ computed barrier (${}^3\text{TS}_2$), much similar to the $13.0 \text{ kcal.mol}^{-1}$ barrier required to afford PhPh from the quaternized homoleptic analogue $[\text{Ph}_4\text{Fe}^{\text{II}}\text{MgBr}(\text{THF})]^-$. Cross-coupling product 2-PhPy is obtained after reductive elimination as a η^4 -ligand to the Fe^0 (formation of ${}^3\text{F-Fe}^0_{\text{PyPh},2\text{Ph}}$) with a strong exothermicity ($14.0 \text{ kcal.mol}^{-1}$ with respect to ${}^3\text{E-Fe}^{\text{II}}_{\text{Py},3\text{Ph}}$).

Therefore, computation of the cross-coupling surface for the formation of 2-phenylpyridine (Scheme 5) shows that the overall catalytic process can be subdivided into 3 steps, summarized in Scheme 7a. The first one, which will be referred to as “transmetallation step” (TM), connects the bis-aryl complex ${}^1\text{B-Fe}^0_{\text{PyCl},2\text{Ph}}$ with the Fe^0 mono-aryl resting state ${}^3\text{A-Fe}^0_{\text{PhPh},\text{Ph}}$, and requires the ΔG_{TM} span ($\Delta G_{\text{TM}} = 6.5 \text{ kcal.mol}^{-1}$). The two other uphill steps involved in the coupling are the oxidative addition (OA) and the reductive elimination (RE), requiring respective computed spans $\Delta G_{\text{OA}}^\ddagger = 11.1 \text{ kcal.mol}^{-1}$ (which corresponds to the free energy difference between ${}^3\text{TS}_1$ and ${}^1\text{B-Fe}^0_{\text{PyCl},2\text{Ph}}$) and $\Delta G_{\text{RE}}^\ddagger = 16.1 \text{ kcal.mol}^{-1}$ (free energy difference between ${}^3\text{TS}_2$ and ${}^3\text{D-Fe}^{\text{II}}_{\text{Py},2\text{Ph}}$). The barriers required for the oxidative addition (OA) and the reductive elimination (RE) are much more energetically-demanding than the fast formation of the pre-complex ${}^1\text{B-Fe}^0_{\text{PyCl},2\text{Ph}}$ (TM). The overall

coupling rate is thus controlled by the rates of the OA and RE elementary steps, which are both first-order in iron, and zeroth-order in Grignard and 2-PyCl. This result is in agreement with the experimental kinetics data discussed earlier (*vide supra*). A simplified catalytic cycle summarizing the computed data is displayed in Scheme 7b.

Scheme 7 : a) DFT-computed surface for the cross-coupling between PhMgCl and 2-PyCl restricted to the sole intermediates controlling the global free energy spans; ground spin states superscripted for each intermediate; b) simplified cross-coupling cycle.



Alternatively, complexes ${}^3\text{D-Fe}^{\text{II}}_{\text{Py},2\text{Ph}}$ and ${}^3\text{E-Fe}^{\text{II}}_{\text{Py},3\text{Ph}}$ can undergo an anion metathesis with an additional equivalent of PhMgCl leading to the release of PyMgCl and to the formation of homoleptic $\text{Ph}_3[\text{Fe}^{\text{II}}]$ or $\text{Ph}_4[\text{Fe}^{\text{II}}]$ intermediates. The latter can then evolve by reductive elimination to afford the bisaryl PhPh and $[\text{Fe}^0]$, which reenters a new cycle. In a general way, this anion metathesis occurring from heteroleptic $\text{Ph}_2(\text{Ar}')[\text{Fe}^{\text{II}}]$ or $\text{Ph}_3(\text{Ar}')[\text{Fe}^{\text{II}}]$ intermediates is expected to be easier for electron-poor Ar' groups, which are much less nucleophiles than Ph^- anion. This explains the noticeable quantities of PhPh reported in Table 1 using PhMgBr as a nucleophile and electron-poor electrophiles (Table 1, Entries 4, 8, 14).

In an attempt to shed light on the origin of the pyridyl ring's substituents effects evidenced experimentally by the Hammett analysis (Figure 5), the evolution of the two energetic spans involved on the surface (that is : global $\Delta G_{\text{TM}} + \Delta G_{\text{OA}}^\ddagger$ span and $\Delta G_{\text{RE}}^\ddagger$ span, see Scheme 7a) with the nature of the 5-pyridyl substituent was also investigated *in silico*. DFT computation shows that the first span, leading overall to the oxidative addition

transition state ${}^3\text{TS}_1$, decreases linearly with the Hammett parameter of the 5-Z substituent, making this step easier for substrates substituted with electron-withdrawing groups (Figure 6a, blue dots). This tendency is confirmed by the computation of the $\Delta G_{\text{TM}} + \Delta G_{\text{OA}}^\ddagger$ span for additional 5-substituted 2-chloropyridines which were not part of the experimental kinetics analysis (Figure 6a, orange dots). Such a result is in line with the classic reactivity trends for oxidative additions, which usually proceed faster for electron-poor derivatives.

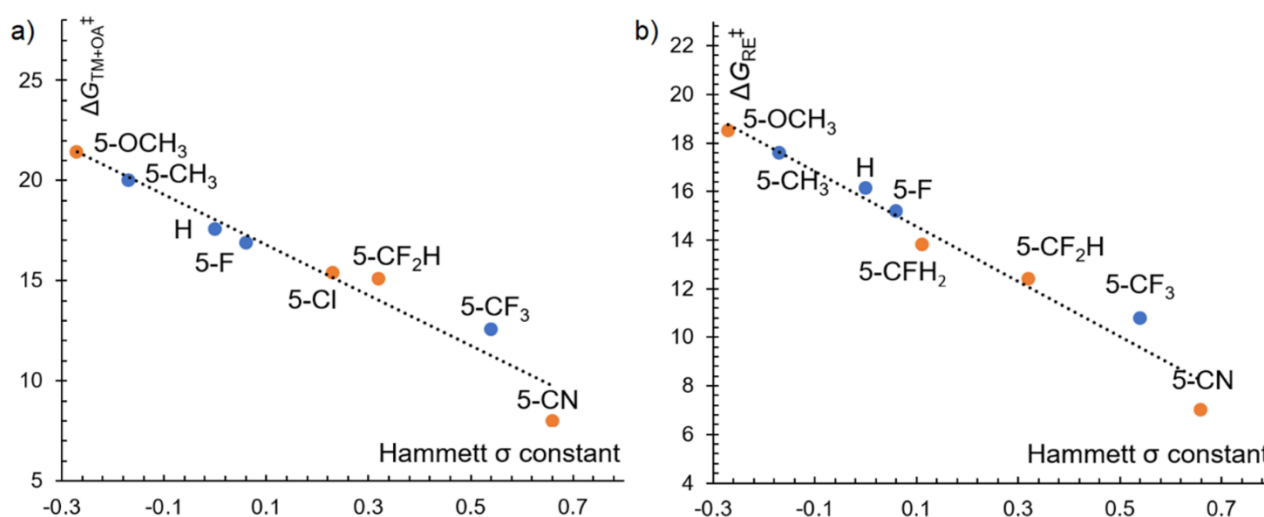


Figure 6 : evolution of the a) $\Delta G_{\text{TM}} + \Delta G_{\text{OA}}^\ddagger$ and b) $\Delta G_{\text{RE}}^\ddagger$ DFT-computed spans with the Hammett parameter of the 5-Z substituent for a series of 2-chloropyridines (blue dots : substrates used in the experimental Hammett plot in Figure 5; orange dots : *in silico* only investigated substrates); spans in kcal.mol⁻¹.

Interestingly, a similar tendency was also observed for the computed reductive elimination span $\Delta G_{\text{RE}}^\ddagger$, which decreased linearly with the Hammett parameter of the 5-Z substituent borne by the pyridyl ring (Figure 6b), suggesting that reductive elimination of the 2-phenylpyridines at the iron(II) proceeds faster for electron-poor pyridyl rings. Reductive elimination of bisaryls often proceeds with increased rates for electron-rich aryl groups, consistently with the stronger reducing power of the latter. A classic example illustrating this tendency was reported by Hartwig, who discussed such substituent effects in the reductive elimination of symmetric bisaryls in diphosphine-ligated platinum (P,P)Pt^{II}(Ar)₂ complexes.^{26a} In the present case, the accelerated reductive elimination rates predicted for electron-poor substituents indicate that the formation of the C—C bond in TS_2 does not occur with a classic synchronous 3-centered mechanism as it is observed for symmetric bis-aryls. It conversely suggests that the reductive elimination transition state involves a migration of the

electron-rich ligand Ph^- onto the electron-poor pyridyl ring. This migration is made easier for pyridyl rings with an increased electron deficiency, hence the lower computed activation barrier for iron(II) intermediates ligated by electron-withdrawing-substituted pyridyl rings (Figure 6b). Similar migratory mechanisms have also been suggested by Hartwig to explain the kinetics trends of C—S bond formation by reductive elimination from Pd^{II} aryl thiolates, which proceeds faster for the combination of electron-rich thiolato ligands and electron-deficient carbon-ligated ligands.^{26b,c} Overall, DFT analysis of the role of the 5-Z substituents of the 2-pyridyl ring shows that both oxidative addition and reductive elimination steps are favored for electron-poor pyridyl derivatives, in agreement with the experimental trends evidenced in Hammett plot (Figure 5). As outlined at the beginning of this section, it must be stated that the DFT calculations discussed herein should be taken only from an informative standpoint, since simplified mechanistic patterns, limited to mononuclear species, have been discussed.

CONCLUSION.

We demonstrated in this work that two strongly different mechanisms can be at work in iron-mediated cross-couplings between aryl Grignard reagents and (hetero)aryl halides. A first mechanism involves *ate*- Fe^{II} species $[\text{Ar}_3\text{Fe}^{\text{II}}]^-$ formed at early stages of the process. In that case, the key step is a single-electron transfer between $[\text{Ar}_3\text{Fe}^{\text{II}}]^-$ and the (hetero)aryl halide, leading to a $\text{Fe}^{\text{II}} / \text{Fe}^{\text{III}}$ coupling sequence. This mechanism is much similar to what has already been reported for related couplings involving alkyl halides, and occurs for (hetero)aryl electrophiles with a high first-reduction potential. An alternative mechanism has also been unveiled for more difficultly reduced substrates. In that case, evolution of $[\text{Ar}_3\text{Fe}^{\text{II}}]^-$ affords transient Fe^0 species, which display cross-coupling catalytic activity and are able to activate (hetero)aryl halides by 2-electron oxidative addition. Heteroleptic species $[\text{Mes}_2(2\text{-Py})\text{Fe}^{\text{II}}]^-$ and $[\text{Mes}_2(\text{C}_6\text{F}_5)\text{Fe}^{\text{II}}]^-$, formed by oxidative addition of Fe^0 onto 2-PyCl and $\text{C}_6\text{F}_5\text{Cl}$ in the presence of MesMgBr , were characterized, sustaining the feasibility of this unprecedented bielectronic mechanism. DFT calculations suggest that the oxidative addition and reductive elimination elementary steps involved in this mechanism are facilitated for electrophilic partners substituted by electron-withdrawing groups, which is supported by experimental Hammett kinetics analysis. Those results highlight the variety of the mechanistic patterns which can be

involved in iron-catalyzed cross-couplings, since in some cases both Fe^{II} / Fe^{III} and Fe⁰ / Fe^{II} sequences can afford the coupling product for a same set of reactants.

AUTHOR INFORMATION

Corresponding Author

*E-mail: guillaume.lefevre@chimieparistech.psl.eu

Notes

The authors declare no competing financial interests.

REFERENCES

- [1] a) Tamura, M.; Kochi, J. K. Vinylation of Grignard reagents. Catalysis by iron. *J. Am. Chem. Soc.* **1971**, *93*, 1487–1489; b) Neumann, S. M.; Kochi, J. K. Synthesis of olefins. Cross-coupling of alkenyl halides and Grignard reagents catalyzed by iron complexes. *J. Org. Chem.* **1975**, *40*, 599–606; c) Cahiez, G.; Avedissian, H. Highly Stereo- and Chemoselective Iron-Catalyzed Alkenylation of Organomagnesium Compounds. *Synthesis* **1998**, *1998*, 1199–1205 ; d) Fürstner, A.; Leitner, A.; Méndez, M.; Krause, H. Iron-Catalyzed Cross-Coupling Reactions. *J. Am. Chem. Soc.* **2002**, *124*, 13856–13863; e) Martin, R.; Fürstner, A. Cross- Coupling of Alkyl Halides with Aryl Grignard Reagents Catalyzed by a Low- Valent Iron Complex. *Angewandte Chemie International Edition* **2004**, *43*, 3955–3957; f) Nakamura, M.; Matsuo, K.; Ito, S.; Nakamura, E. Iron-Catalyzed Cross-Coupling of Primary and Secondary Alkyl Halides with Aryl Grignard Reagents. *J. Am. Chem. Soc.* **2004**, *126*, 3686–3687; g) Hatakeyama, T.; Hashimoto, T.; Kondo, Y.; Fujiwara, Y.; Seike, H.; Takaya, H.; Tamada, Y.; Ono, T.; Nakamura, M. Iron-Catalyzed Suzuki–Miyaura Coupling of Alkyl Halides. *J. Am. Chem. Soc.* **2010**, *132*, 10674–10676; h) Bedford, R. B.; Huwe, M.; Wilkinson, M. C. Iron-catalysed Negishi coupling of benzylhalides and phosphates. *Chem. Commun.* **2009**, *0*, 600–602; i) Bedford, R. B.; Brenner, P. B.; Carter, E.; Cogswell, P. M.; Haddow, M. F.; Harvey, J. N.; Murphy, D. M.;

Nunn, J.; Woodall, C. H. TMEDA in Iron- Catalyzed Kumada Coupling: Amine Adduct versus Homoleptic “ate” Complex Formation. *Angew. Chem. Int. Ed.* **2014**, *53*, 1804–1808.

[2] a) R. B. Bedford, P. B. Brenner, The development of iron catalysts for cross-coupling reactions. *Iron Catalysis II*; Bauer, E., Ed.; Springer Intl., 2015; b) for a recent report of some by us about an iron-catalyzed cross-coupling using cheap and non-toxic alkoxide ligands, see : Cahiez, G.; Lefèvre, G.; Moyeux, A.; Guerret, O.; Gayon, E.; Guillonnet, L.; Lefèvre, N.; Gu, Q.; Zhou, E. Gram-scale, Cheap, and Eco-friendly Iron-catalyzed Cross-Coupling between Alkyl Grignard reagents and Alkenyl or Aryl halides. *Org. Lett.* **2019**, *21*, 2679-2683.

[3] a) Carpenter, S. H.; Neidig, M. L. A Physical-Inorganic Approach for the Elucidation of Active Iron Species and Mechanism in Iron-Catalyzed Cross-Coupling. *Isr. J. Chem.* **2017**, *57*, 1106-1116; b) Sears, J. D.; Neate, P. G. N.; Neidig, M. L. Intermediates and Mechanism in Iron-Catalyzed Cross-Coupling. *J. Am. Chem. Soc.* **2018**, *140*, 11872-11883; c) Neidig, M. L.; Carpenter, S. H.; Curran, D. J.; DeMuth, J. C.; Fleischauer, V. E.; Iannuzzi, T. E.; Neate, P. G. N.; Sears, J. D.; Wolford, N. J. Development and Evolution of Mechanistic Understanding in Iron-Catalyzed Cross-Coupling. *Acc. Chem. Res.* **2019**, *52*, 140-150.

[4] For a recent review on iron-mediated radical processes, see Kyne, S. H.; Lefèvre, G.; Ollivier, C.; Petit, M.; Ramis Cladera, V.-A.; Fensterbank, L. Iron and cobalt catalysis: new perspectives in synthetic radical chemistry. *Chem. Soc. Rev.*, **2020**, *49*, 8501-8542.

[5] Seidel, V. W.; Lattermann, K.-J. Trimesitylferrate und Komplexbildung mit P-Donoren. *Z. anorg. allg. Chem.* **1982**, *488*, 69-74.

[6] a) Lefèvre, G.; Jutand, A. Activation of Aryl and Heteroaryl Halides by an Iron(I) Complex Generated in the Reduction of [Fe(acac)₃] by PhMgBr: Electron Transfer versus Oxidative Addition. *Chem. Eur. J.* **2014**, *20*, 4796-4805; b) Clémancey, M.; Cantat, T.; Blondin, G.; Latour, J.-M.; Dorlet, P.; Lefèvre, G. Structural Insights into the Nature of Fe⁰ and Fe^I Low-Valent Species Obtained upon the Reduction of Iron Salts by Aryl Grignard Reagents. *Inorg. Chem.* **2017**, *56*, 3834-3848; c) Rousseau, L.; Herrero, C.; Clémancey, M.; Imberdis, A.; Blondin, G.; Lefèvre, G. Evolution of Ate-Organoniron(II) Species towards Lower Oxidation States: Role of the Steric and Electronic Factors. *Chem. Eur. J.* **2020**, *26*, 2417-2428.

- [7] Sun, C.; Krause, H.; Fürstner, A. A Practical Procedure for Iron-Catalyzed Cross-Coupling Reactions of Sterically Hindered Aryl-Grignard Reagents with Primary Alkyl Halides. *Adv. Synth. Catal.* **2014**, *356*, 1281–1291.
- [8] a) Hatakeyama, T.; Fujiwara, Y.; Okada, Y.; Itoh, T.; Hashimoto, T.; Kawamura, S.; Ogata, K.; Takaya, H.; Nakamura, M. Kumada-Tamao-Corriu Coupling of Alkyl Halides Catalyzed by an Iron-Bisphosphine Complex. *Chem. Lett.* **2011**, *40*, 1030–1032; b) Daifuku, S. L.; Al-Afyouni, M. H.; Snyder, B. E. R.; Kneebone, J. L.; Neidig, M. L. A Combined Mössbauer, Magnetic Circular Dichroism, and Density Functional Theory Approach for Iron Cross-Coupling Catalysis: Electronic Structure, In Situ Formation, and Reactivity of Iron-Mesityl-Bisphosphines. *J. Am. Chem. Soc.* **2014**, *136*, 9132.
- [9] For a complete review on Fe-catalyzed cross-couplings, see Bauer, I.; Knölker, H.-J. Iron Catalysis in Organic Synthesis. *Chem. Rev.* **2015**, *115*, 3170–3387, section 2.4.1.
- [10] Blanksby, S. J.; Ellison, G. B. Bond Dissociation Energies of Organic Molecules. *Acc. Chem. Res.* **2003**, *36*, 255.
- [11] Hatakeyama, T.; Hashimoto, S.; Ishizuka, K.; Nakamura, M. Highly Selective Biaryl Cross-Coupling Reactions between Aryl Halides and Aryl Grignard Reagents: A New Catalyst Combination of N-Heterocyclic Carbenes and Iron, Cobalt, and Nickel Fluorides. *J. Am. Chem. Soc.* **2009**, *131*, 11949–11963.
- [12] a) Enemaerke, R. J.; Christensen, T. B.; Jensen, H.; Daasbjerg, K. Application of a New Kinetic Method in the Investigation of Cleavage Reactions of Haloaromatic Radical Anions. *J. Chem. Soc., Perkin Trans. 2* **2001**, 1620–1630; b) Ji, C.; Peters, D. G.; Davidson, E. R. Electrochemical Reduction of Halogenated Pyrimidines at Mercury Cathodes in Acetonitrile. *J. Electroanal. Chem.* **2001**, *500*, 3–11; c) Andrieux, C. P.; Savéant, J.-M.; Zann, D. Relationship between reduction potentials and cleavage rates in aromatic molecules. *Nouv. J. Chim.* **1984**, *8*, 107–116; d) Muthukrishnan, A.; Sangaranarayanan, M. V. Mechanistic Analysis of the Reductive Cleavage of Carbon–Halogen Bonds in Halopentafluorobenzenes. *J. Electrochem. Soc.* **2009**, *156*, 23–28.
- [13] Wu, W.; Teng, Q.; Chua, Y.; Huynh, H. V.; Duong, H. A. Iron-Catalyzed Cross-Coupling Reactions of Arylmagnesium Reagents with Aryl Chlorides and Tosylates: Influence of Ligand Structural Parameters and Identification of a General N-Heterocyclic Carbene Ligand. *Organometallics* **2017**, *36*, 12, 2293–2297.

- [14] Tachiya, M. Generalization of the Marcus equation for the electron-transfer rate. *J. Phys. Chem.* **1993**, *97*, 22, 5911–5916.
- [15] ¹H NMR data for [Mes₂Fe^{II}Br][−] were in agreement with those reported by Bedford, see reference 1i.
- [16] The *o*-CH₃ protons of mesityl-Fe^{II} high-spin complexes usually display a broad signal in the 20-30 ppm area; it is not excluded that the corresponding *o*-CH₃ protons are responsible of the broad shoulder at ca. 20 ppm. However, the poor signal-to-noise ratio of the spectrum in this area precludes a more accurate assignment; see Hawrelak, E. J.; Bernskoetter, W. H.; Lobkovsky, E.; Yee, G. T.; Bill, E.; Chirik, P. J. Square Planar vs Tetrahedral Geometry in Four Coordinate Iron(II) Complexes. *Inorg. Chem.* **2005**, *44*, 3103-3111.
- [17] For recent examples of ¹H NMR characterized high-spin phenyliron(II) species, see a) Werncke, C. G.; Pfeiffer, J.; Müller, I.; Vendier, L.; Sabo-Etienne, S.; Bontemps, S. C-Halide bond cleavage by a two-coordinate iron(i) complex. *Dalton Trans.* **2019**, *48*, 1757-1765; b) Rousseau, L.; Touati, N.; Binet, L.; Thuéry, P.; Lefèvre, G. Relevance of single-transmetallated resting states in iron-mediated cross-couplings: unexpected role of σ -donating additives. *Inorg. Chem.* **2021**, *60*, 7991–7997.
- [18] a) Hill, D. H.; Parvez, M. A.; Sen, A. Mechanistic Aspects of the Reaction of Anionic Iron(0)-Olefin Complexes with Organic Halides. Detection and Characterization of Paramagnetic Organometallic Intermediates. *J. Am. Chem. Soc.* **1994**, *116*, 7, 2889–2901; b) Koch, D. A., Henne, B. J., Bartak, D. E. Carbanion and Radical Intermediacy in the Electrochemical Reduction of Benzyl Halides in Acetonitrile. *J Electrochem Soc.* **1987**, *134*, 3062; c) Cahiez, G.; Habiak, V.; Duplais, C.; Moyeux, A. Iron- Catalyzed Alkylations of Aromatic Grignard Reagents. *Angew. Chem. Int. Ed.* **2007**, *46*, 4364.
- [19] Parchomyk, T.; Koszinowski, K. Ate Complexes in Iron- Catalyzed Cross- Coupling Reactions. *Chem. Eur. J.* **2016**, *22*, 15609–15613.
- [20] Bauer, G.; Wodrich, M. D.; Scopelliti, R.; Hu, X. Iron Pincer Complexes as Catalysts and Intermediates in Alkyl–Aryl Kumada Coupling Reactions. *Organometallics* **2015**, *34*, 1, 289–298.
- [21] Cotton, F. A.; Luck, R. L.; Son, K. New Polynuclear Compounds of Iron(II) Chloride with Oxygen Donor Ligands Part I. Fe₄Cl₈(THF)₆: Synthesis and a Single Crystal X-ray Structure Determination. *Inorg. Chim. Acta* **1991**, *179*, 11–15.
- [22] a) Gaussian 09, Revision D.01, M. J. Frisch *et al.*, Gaussian, Inc., Wallingford CT, 2013; b) Swart, M.; Ehlers, A. W.; Lammertsma, K. Performance of the OPBE Exchange-Correlation Functional. *Mol. Phys.*

2004, *102*, 2467–2474; c) Swart, M.; Groenhof, A. R.; Ehlers, A. W.; Lammertsma, K. Validation of Exchange–Correlation Functionals for Spin States of Iron Complexes. *J. Phys. Chem. A* **2004**, *108*, 25, 5479–5483; d) Swart, M. Accurate Spin-State Energies for Iron Complexes. *J. Chem. Theory Comput.* **2008**, *4*, 12, 2057–2066; e) S. Miertus, E. Scrocco, J. Tomasi Electrostatic interaction of a solute with a continuum. A direct utilization of AB initio molecular potentials for the prevision of solvent effects, *Chem. Phys.* **1981**, *55*, 117–129; f) G. Scalmani, M. J. Frisch, B. Mennucci, J. Tomasi, R. Cammi, V. Barone Geometries and properties of excited states in the gas phase and in solution: Theory and application of a time-dependent density functional theory polarizable continuum model, *J. Chem. Phys.* **2006**, *124*, 094107.

[23] Zhurkin, F. E.; Wodrich, M. D.; Hu, X. A Monometallic Iron(I) Organoferrate. *Organometallics* **2017**, *36*, 3, 499–501.

[24] For a recent example of structurally characterized *tris*- η^2 -styrene-ligated *ate*-Fe⁰ alkyl species, see Neate, P. G. N.; Greenhalgh, M. D.; Brennessel, W. W.; Thomas, S. P.; Neidig, M. L. TMEDA in Iron- Catalyzed Hydromagnesiation: Formation of Iron(II)- Alkyl Species for Controlled Reduction to Alkene- Stabilized Iron(0). *Angew. Chem. Int. Ed.* **2020**, *59*, 17070–17076.

[25] Rousseau, L.; Brémond, E.; Lefèvre, G. Assessment of the ground spin state of iron(I) complexes: insights from DFT predictive models. *New J. Chem.*, **2018**, *42*, 7612–7616.

[26] a) Shekhar, S.; Hartwig, J. F. Distinct Electronic Effects on Reductive Eliminations of Symmetrical and Unsymmetrical Bis-Aryl Platinum Complexes. *J. Am. Chem. Soc.* **2004**, *126*, 13016–13027; b) Mann, G.; Baranano, D.; Hartwig, J. F.; Rheingold, A. L.; Guzei, I. A. Carbon–Sulfur Bond-Forming Reductive Elimination Involving sp-, sp²-, and sp³-Hybridized Carbon. Mechanism, Steric Effects, and Electronic Effects on Sulfide Formation. *J. Am. Chem. Soc.* **1998**, *120*, 36, 9205–9219; c) In order to strengthen those theoretical predictions with robust experimental data regarding the effect of the pyridyl substituents on the kinetics of the reductive elimination, stoichiometric Hammett kinetics analysis would undoubtedly be of high interest. However, well-defined heteroleptic diaryliron(II) species are difficultly prepared and their intrinsic thermal instability makes extremely complex a kinetic monitoring of their evolution towards the formation of Fe⁰ and bisaryls, unlike some of their Pd^{II} analogues. Such an approach was followed by Hartwig and Buchwald, who respectively used room-temperature-stable diphosphine-ligated Pd^{II} aryl thiolates and RuPhos-ligated Pd^{II} aryl amides to access kinetics parameters of C–S and C–N bond formation by thermally-induced reductive

elimination from those species - see ref. 26b and: Arrechea, P. L.; Buchwald, S. L. Biaryl Phosphine Based Pd(II) Amido Complexes: The Effect of Ligand Structure on Reductive Elimination. *J. Am. Chem. Soc.* **2016**, *138*, 38, 12486–12493.

ASSOCIATED CONTENT

Supporting information (PDF): general procedures, ^1H NMR spectra, theoretical methods, cartesian coordinates of the computed structures. The corresponding files are available free of charge.

Author Contributions

The manuscript was written through contributions of all authors. All authors have given approval to the final version of the manuscript.

Funding Sources

G.L. thanks the ANR (Project JCJC SIROCCO), the ERC (Project DoReMI StG, 852640) and the CNRS (Project IrMaCAR) for their financial support. The NMR shared facilities of Chimie ParisTech (Dr. M.-N. Rager) are thanked for technical support.

For table of contents only

